

HOSTED BY



Contents lists available at ScienceDirect

Journal of King Saud University – Science

journal homepage: [www.sciencedirect.com](http://www.sciencedirect.com)

Original article

# Cytotoxicity and apoptosis induction of copper oxide-reduced graphene oxide nanocomposites in normal rat kidney cells



Rashid Lateef<sup>a,b</sup>, Marhaba<sup>a,c</sup>, Payal Mandal<sup>a</sup>, Kausar M. Ansari<sup>a,c</sup>, Mohd Javed Akhtar<sup>d</sup>, Maqusood Ahamed<sup>d,\*</sup>

<sup>a</sup> Food Toxicology Laboratory, Food, Drug, and Chemical Toxicology Group, CSIR-Indian Institute of Toxicology Research, Vishvighyan Bhawan, 31, Mahatma Gandhi Marg, Lucknow 226001, Uttar Pradesh, India

<sup>b</sup> Department of Biochemistry, Faculty of Science, Veer Bahadur Singh Purvanchal University, Jaunpur 222003, Uttar Pradesh, India

<sup>c</sup> Academy of Scientific and Innovative Research (AcSIR), Ghaziabad 201002, India

<sup>d</sup> King Abdullah Institute for Nanotechnology, King Saud University, Riyadh 11451, Saudi Arabia

## ARTICLE INFO

### Article history:

Received 13 October 2022

Revised 3 November 2022

Accepted 14 December 2022

Available online 21 December 2022

### Keywords:

CuO-rGO

NRK52E cells

ROS

Chromosomal condensation

Acridine orange/ethidium bromide

Cell cycle

## ABSTRACT

Copper oxide-reduced graphene oxide nanocomposites (CuO-rGO NCs) have received great attention from researchers due to their exceptional physicochemical properties that cannot be achieved by a single composition. CuO-rGO NCs have the potential to be used in diverse fields including agriculture, cosmetic, textile, the food industry, and biomedicine. The growing application and production of CuO-rGO NCs raises the concern of their effects on human and the environmental health. Knowledge on the toxicological response of CuO-rGO NCs in biological systems is scarce. This study was aimed to explore the cytotoxicity and apoptosis response of CuO-rGO NCs in normal rat kidney cells (NRK52E). CuO-rGO NCs was synthesized by a simple hydrothermal method using copper nitrate and graphene oxide (GO) as precursors. X-ray diffraction (XRD), field emission scanning electron microscopy (FESEM), and energy dispersive X-ray spectroscopy (EDS) confirmed the preparation of CuO-rGO NCs with high crystallinity, polygonal shape, smooth surface morphology. Besides, CuO nanoparticles were tightly anchored on rGO nanosheets. Biological results showed that CuO-rGO NCs induce a dose-dependent cytotoxicity in NRK52E cells evident by cell viability reduction and irregular cellular morphology. Fluorescent microscopic examination of 2,7-dichlorofluorescein probe showed that CuO-rGO NCs generate intracellular reactive oxygen species (ROS) in NRK52E cells. Acridine orange/ethidium bromide dual staining depicted that number of orange-red stained cells (apoptotic cells) increases with increasing concentration of CuO-rGO NCs. The 4', 6-diamidino-2-phenylindole (DAPI) fluorescent staining exhibited that CuO-rGO NCs induce chromosomal condensation while normal-shaped nuclei were observed in the control cells. In cell cycle analysis, cells exposed to CuO-rGO NCs demonstrated significantly higher accumulation of apoptotic cells in subG1 phase. Altogether, we observed that CuO-rGO NCs induce cytotoxicity, ROS generation, and apoptosis in NRK52E cells. This preliminary study warrants future research to evaluate the potential mechanisms of CuO-rGO NCs toxicity at molecular level.

© 2022 The Author(s). Published by Elsevier B.V. on behalf of King Saud University. This is an open access article under the CC BY-NC-ND license (<http://creativecommons.org/licenses/by-nc-nd/4.0/>).

\* Corresponding author.

E-mail address: [mahamed@ksu.edu.sa](mailto:mahamed@ksu.edu.sa) (M. Ahamed).

Peer review under responsibility of King Saud University.



Production and hosting by Elsevier

## 1. Introduction

Nanotechnology commonly refers to the creation, manipulation, and application of materials, structures, or devices with at least one dimension in the 1–100 nm range (Ahamed et al., 2015). Nanostructures of metal oxides including copper oxide nanoparticles (CuO NPs) are being used in a number of products, and their applications are anticipated to expand in coming years (Cuillel et al., 2014; Sruthi et al., 2018). According to a recent report, global consumption of CuO NPs will increase by 200–800 tons per year between 2020 and 2025 (Yang et al., 2020). Due to

<https://doi.org/10.1016/j.jksus.2022.102513>

1018-3647/© 2022 The Author(s). Published by Elsevier B.V. on behalf of King Saud University.

This is an open access article under the CC BY-NC-ND license (<http://creativecommons.org/licenses/by-nc-nd/4.0/>).

unique physicochemical properties CuO NPs are being used as catalysts, batteries, solar energy, photovoltaic cells, and heat transfer nanofluids (Nayak et al., 2020; Sarker et al., 2021). CuO NPs are also utilized in paints, plastics, food containers, textiles, and biomedicine because of their antimicrobial activity (Ahamed et al., 2014; Azam et al., 2012). There is no dispute in the fact that CuO NPs pose a serious threat to the environment and to people who come into contact with them (Wu et al., 2020; Xu et al., 2017). Therefore, the health safety of CuO NP exposure has moved to the top concern for regulatory and scientific bodies (Naz et al., 2020). The toxicological profile of CuO NPs has been reported through several *in vitro* and *in vivo* studies at the cellular and molecular level (Bugata et al., 2019; Siddiqui et al., 2013; Zhang et al., 2018). The mechanistic approach suggested that CuO NPs induced inflammation, cytotoxicity, DNA damage, and apoptosis through the generation of reactive oxygen species (ROS) and oxidative stress (Abdelazeim et al., 2020; Baeg et al., 2018).

Recent studies have concentrated on enhancing the physicochemical characteristics of CuO NPs. The physicochemical properties of CuO NPs can be tuned through various methods including doping with metal ions and creating nanohybrids and nanocomposites (NCs) (Arun et al., 2020; Islam et al., 2020). CuO NPs and graphene derivatives-based nanocomposites (NCs) are being produced by researchers because of their inherently superior properties that cannot be achieved by a single composition (Zhang et al., 2016). Graphene oxide (GO) and reduced graphene oxide (rGO) are two important graphene derivatives that have received a lot of attention over the last decade because of their unique structure and incredible properties such as high thermal, electrical, and mechanical strength (Padmajan Sasikala et al., 2018). The high surface area with a large number of oxygen functional groups and surface defects enables GO/rGO for various purposes e.g. nanohybrids/nanocomposites, sensors, fuel cells, supercapacitors, and biomedicine (Ahamed et al., 2022, 2021; Shewale and Yun, 2020). Recent studies observed that CuO-rGO demonstrate better antimicrobial activity than individual components (Rajapaksha et al., 2019; Siddique et al., 2021).

The growing application of CuO-rGO NCs raises the concern of their impacts on human body. The suitability of nanostructures for utilization in a wide range of products, including biomedical, must be supported by extensive research on their potential health hazards. Investigations into the toxicological potential of CuO-rGO NCs are scarce. This study was aimed to investigate the cytotoxicity and apoptosis induction of CuO-rGO NCs in normal rat kidney cells (NRK52E). CuO-rGO NCs was prepared through a facile hydrothermal procedure utilizing copper nitrate and GO as precursors. Preparation of CuO-rGO NCs was confirmed by X-ray diffraction (XRD), field emission scanning electron microscopy (FESEM) and energy dispersive X-ray spectroscopy (EDS). Cytotoxicity of CuO-rGO NCs was examined by cell viability assays (MTT and trypan blue) and cellular morphology. Intracellular generation of reactive oxygen species (ROS) following CuO-rGO NCs exposure was assessed by a fluorescent microscope using 2,7-dichlorofluorescein diacetate (DCFH-DA) probe. CuO-rGO NCs induced chromosomal condensation was examined utilizing 4', 6-diamidino-2-phenylindole (DAPI) staining. Acridine orange/ ethidium bromide (AO/EB) double staining was applied to evaluate apoptosis response of CuO-rGO NCs using fluorescent microscope. Cell cycle progression was examined by flow cytometer using propidium iodide (PI).

## 2. Materials and methods

### 2.1. Synthesis of CuO-rGO NCs

CuO-rGO NCs was synthesized by a simple hydrothermal method using copper nitrate ( $\text{CuNO}_3 \cdot 2\text{H}_2\text{O}$ ) (Sigma-Aldrich, St.

Louis, MO, USA) and GO (Sigma-Aldrich) as starting materials. Initially, 0.1 g of GO was dispersed into 100 ml of de-ionized water and sonicated for 2 h to obtain a uniform suspension. The 0.1 M copper nitrate was dissolved in 100 ml of de-ionized water in a separate flask. Then, 50 ml of GO suspension was added into 50 ml of copper nitrate solution and stirred for 1 h. The pH of the reaction mixture was maintained 11 through dropwise addition of NaOH (0.04 M). The reaction mixture was further transferred into a Teflon-coated autoclave and heated at 120 °C for 5 h to get black precipitates. At the end, precipitate was washed and dried at 120 °C for 5 h to get CuO-rGO NCs.

### 2.2. Characterization of CuO-rGO NCs

Crystallinity and phase purity of CuO-rGO NCs was examined at X-ray diffraction (XRD) (PanAnalytic X Pert Pro) (Malvern Instruments, WR14 1XZ, UK) using Cu-K $\alpha$  radiation ( $\lambda = 0.154 \text{ nm}$  at 45 kV and 40 mA). Structural characterization was further carried out by field emission scanning electron microscopy (FESEM, JSM-7600F, JEOL, Inc., Tokyo, Japan). Elemental composition and elemental mapping were examined at energy dispersive X-ray spectroscopy (EDS) associated with FESEM.

### 2.3. Cell culture

Normal rat kidney cell line (NRK52E, ATCC No. CRL1571) was obtained from American Type Culture Collection (ATCC, Virginia, USA). Cells were cultured in Dulbecco's Modified, Eagle Medium (DMEM, Carlsbad, CA, USA) with high glucose and supplemented with 10 % fetal bovine serum (FBS), 13.5 g/L sodium bicarbonate, and antibiotic-antimycotic solution (50 unit/ml Penicillin, 50  $\mu\text{g}/\text{ml}$  Streptomycin, and 0.25  $\mu\text{g}/\text{ml}$  Amphotericin-B). Cells were maintained at 37 °C in a humidified incubator with 5 %  $\text{CO}_2$  supply.

### 2.4. Exposure of CuO-rGO to NRK52E cells

CuO-rGO NCs was suspended in de-ionized water to prepare a stock suspension (1 mg/ml). The stock suspension was further diluted in DMEM to get the desired concentration of CuO-rGO NCs for exposure to NRK52E cells. Cells were treated to different concentrations (1–200  $\mu\text{g}/\text{ml}$ ) CuO-rGO NCs for 24 h. Cells without CuO-rGO NCs served as the negative control in each experiment. For ROS estimation  $\text{H}_2\text{O}_2$  was used as a positive control.

### 2.5. Assay of cytotoxicity, ROS, and apoptosis parameters

MTT cell viability assay was performed according to the method of Mossman (Mosmann, 1983). Trypan blue dye exclusion assay was also carried out for cytotoxicity estimation (Strober, 2015). Morphology of control and CuO-rGO NCs exposed cells was examined at an inverted phase-contrast microscope. Microscopic visualization of intracellular ROS generation following exposure to different concentrations of CuO-rGO NCs for 24 h was carried out using the fluorescent probe 2,7-dichlorofluorescein diacetate (DCFH-DA) (Sigma Aldrich) as reported earlier (Wang and Joseph, 1999). Nucleus morphology of control and CuO-rGO NCs treated cells was assessed using a 4', 6-diamidino-2-phenylindole (DAPI) (Sigma-Aldrich), which binds to the adenine-thymine-rich region of DNA. In brief, DAPI solution (1 mg/ml) was used to stain the control and treated cells and incubated for 10 min in dark at 37 °C. DAPI-stained fluorescent nuclei images were grabbed with a Leica DCF 295 camera using a Leica DM 100 microscope (Nussloch, Germany). Acridine orange/ethidium bromide (AO/EB, Sigma-Aldrich) dual fluorescent staining was applied to examine the apoptotic response of CuO-rGO NCs in NRK52E cells. Briefly,  $20 \times 10^4$  cells/well were seeded in 12-well plate and exposed to 10  $\mu\text{g}/\text{ml}$  and

25  $\mu\text{g/ml}$  of CuO-rGO NCs for 24 h. After the completion of incubation period, cells were washed with PBS and added the 2  $\mu\text{l}$  dual fluorescent staining solution (100  $\mu\text{g/ml}$  AO and 100  $\mu\text{g/ml}$  of EB) to each well. Then, morphology of apoptotic cells was evaluated within 20 min at a fluorescent microscope (Leica DM 100). Cell cycle progression of NRK52E cells exposed to different concentrations of CuO-rGO NCs (1–10  $\mu\text{g/ml}$  for 24 h) were analysed by the flow cytometer (BD Influx™ Cell Sorter) using propidium iodide (PI).

### 2.6. Statistical analysis

One-way analysis of variance (ANOVA) followed by Dunnett's multiple comparison test was carried out to examine the statistical significance of quantitative data. The p value < 0.05 was credited as statistical significance.

## 3. Results and discussion

### 3.1. XRD, FESEM, and EDS characterization of CuO-rGO NCs

XRD, FESEM, and EDS techniques were applied to confirm the synthesis of CuO-rGO NCs. Fig. 1 demonstrated the XRD spectra of CuO-rGO NCs. All the diffraction peaks observed at  $2\theta$  were corresponding to the crystal planes (110), (002), (111), (202), (020), (202), (113), (311), and (220) that suggest the formation of monoclinic structure of CuO according to Joint Committee on Powder Diffraction Standards (JCPDS) card no. 45-0937 (Arun et al., 2020). Absence of impurity peaks in XRD spectra suggested the preparation of highly pure CuO-rGO NCs. The sharp and high-intensity peaks of diffraction spectra indicate the good crystallinity of CuO-rGO NCs. The rGO peaks were not appeared in CuO-rGO NCs. This might be due to the homogeneous distribution of CuO NPs on the surface of rGO nanosheets that prevented the restacking of sheets (Ahamed et al., 2021). The crystallite size of CuO-rGO NCs was estimated corresponding to the most prominent peak (111) applying Scherrer's equation (Patterson, 1939). The crystallite size of CuO-rGO NCs was around 45 nm. The surface morphology, shape, and size of prepared CuO-rGO NCs were further characterized by FESEM. The FESEM micrographs exhibited that CuO NPs were in polygonal shape with smooth surface morphology, and tightly anchored on the rGO nanosheets (Fig. 2A and B). The average particle size of CuO-rGO NCs calculated from FESEM was around 43 nm, which was almost similar to the size estimated from XRD. Chemical composition and elemental mapping of CuO-rGO NCs were further examined by energy dispersive X-ray spectroscopy (EDS) associated with FESEM. Fig. 2C shows the weight and atomic percentage of Cu, O, and C elements present in CuO-rGO NCs. Other elemental impurities were not detected in EDS analysis that further supports XRD data. Elemental mapping further indicates the uniform distribution of Cu, O, and C elements in CuO-rGO NCs (Fig. 3). The characterization data of CuO-rGO NCs observed in this study was according to earlier published works (Dat et al., 2022; Zhang et al., 2017).

### 3.2. Cytotoxic response of CuO-rGO NCs

Cells were treated for 24 h with the various concentrations (0, 1, 5, 10, 25, 50, 100, and 200  $\mu\text{g/ml}$ ) of CuO-rGO NCs and cell viability was assessed by MTT and trypan blue assays. These assays are sensitive and integrated tests for assessing the cytotoxicity and cell integrity against drugs, chemicals, and nanostructures (Ghasemi et al., 2021; Strober, 2015). Results of the both assays showed that CuO-rGO NCs induce a dose-dependent cytotoxicity in rat kidney

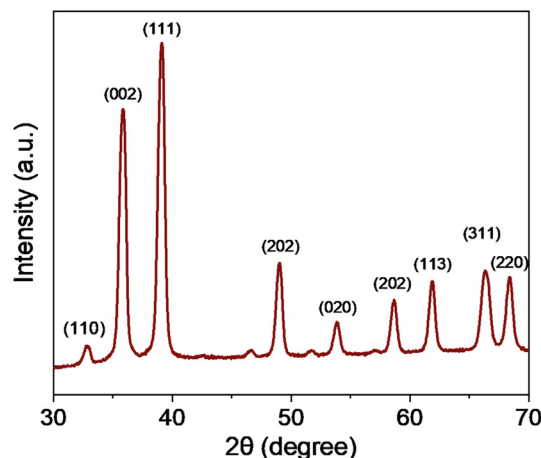


Fig. 1. XRD spectra of CuO-rGO NCs. XRD: X-ray diffraction and CuO-rGO NCs: Copper oxide-reduced graphene oxide nanocomposites.

NRK52E cells. MTT data demonstrated that cell viability reduced to 86 %, 55 %, 49 %, 16 %, 8 %, 3 %, and 3 % upon treatment of CuO-rGO NCs for the concentrations of 1, 2, 5, 10, 25, 50, 100, and 200  $\mu\text{g/ml}$ , respectively (Fig. 4A). The  $\text{IC}_{50}$  value of CuO-rGO NCs calculated from MTT assay was 9  $\mu\text{g/ml}$ . Cytotoxicity data obtained by trypan blue dye exclusion assay support the MTT results. In trypan blue assay, cell viability decreased to 88 %, 57 %, 52 %, 20 %, 12 %, 7 %, and 4 % after exposure to CuO-rGO NCs at the concentrations of 1, 2, 5, 10, 25, 50, 100, and 200  $\mu\text{g/ml}$ , respectively (Fig. 4B). The  $\text{IC}_{50}$  value of CuO-rGO NCs estimated from trypan blue assay was 8.2  $\mu\text{g/ml}$ . To confirm the cell viability data, we further examined morphology of NRK53E cells following exposure to CuO-rGO NCs at the concentrations of 25, 50, and 100  $\mu\text{g/ml}$  for 24 h. Fig. 5 exhibited that CuO-rGO NCs exposure induce cell death in a dose-dependent manner. Phase-contrast inverted micrographs depicted that cells of control group were healthy, with normal morphology, and attached on the surface whereas cells in treated groups displayed irregular morphology, floated in culture medium, and lowering of cell density with significant number of dead cells. These findings indicated that CuO-rGO NCs has potential to exert dose-dependent cytotoxicity in NRK52E cells. In earlier research, it was reported that pure CuO NPs induce cytotoxicity in various types of mammalian cells (Fahmy et al., 2020; Laha et al., 2014). A recent study also found the strong cytotoxic activity of CuO-rGO NCs against human colon cancer (HCT116) cells (Ganesan et al., 2020).

### 3.3. Oxidative stress response of CuO-rGO NCs

Oxidative stress has been suggested as one of the potential mechanisms of nanostructure-induced toxicity in biological systems (Fahmy et al., 2020). This could be due to tiny size and higher surface area of nanostructures that usually induce intracellular ROS generation (Ahamed et al., 2015). ROS also act as signalling molecules to elicit several cellular events such as inflammation, genotoxicity, and apoptosis (Abdelazeim et al., 2020). ROS-induced oxidative stress has been also associated with several human diseases including heart disease, renal disease, and cancer (Sárközy et al., 2018). In order to examine the ROS generating potential of CuO-rGO NCs, NRK52E cells were treated for 24 h to 10  $\mu\text{g/ml}$  and 25  $\mu\text{g/ml}$  of CuO-rGO NCs. Hydrogen peroxide ( $\text{H}_2\text{O}_2$ ) was used as a positive control. The DCFH-DA dye was applied to visualize the ROS levels in NRK52E cells. The DCFH-DA

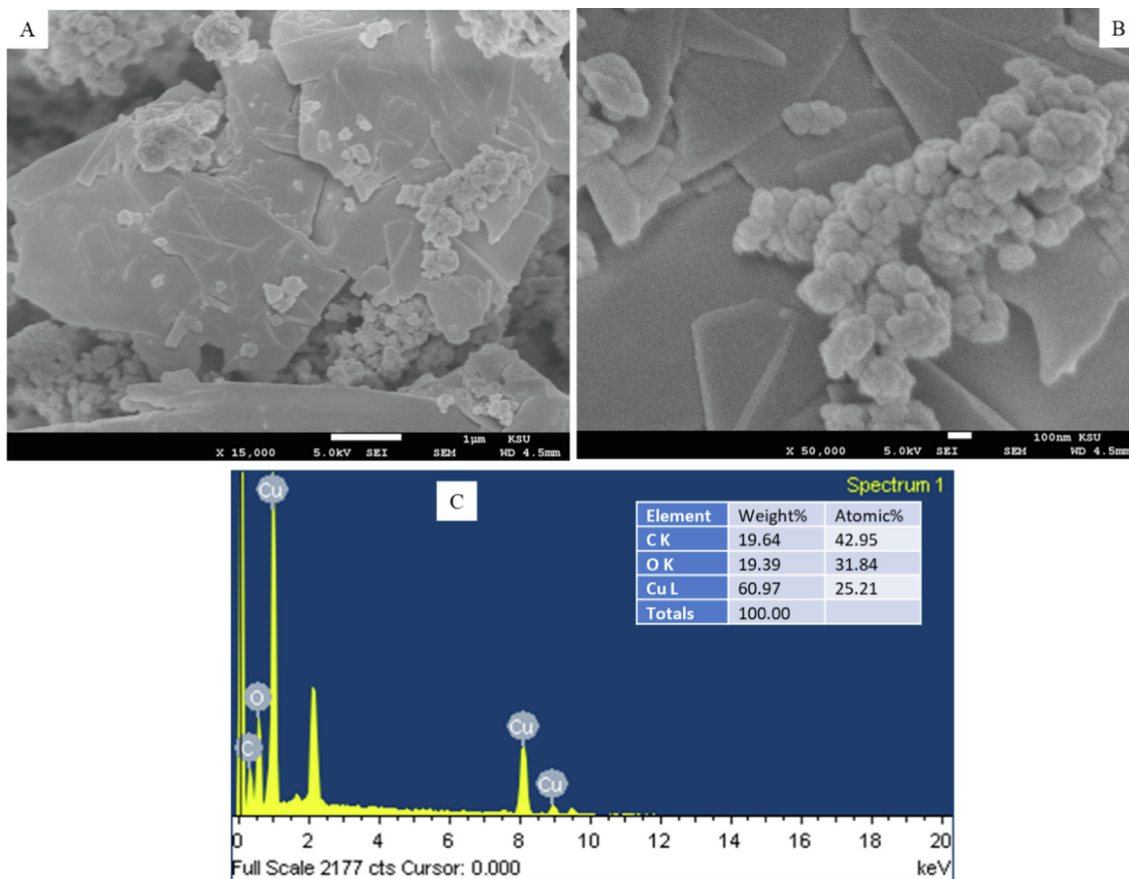


Fig. 2. (A and B) FESEM micrographs and (C) elemental composition of CuO-rGO NCs analysed EDS. FESEM: Field emission scanning electron microscopy, CuO-rGO NCs: Copper oxide-reduced graphene oxide nanocomposites, and EDS: Energy dispersive X-ray spectroscopy.

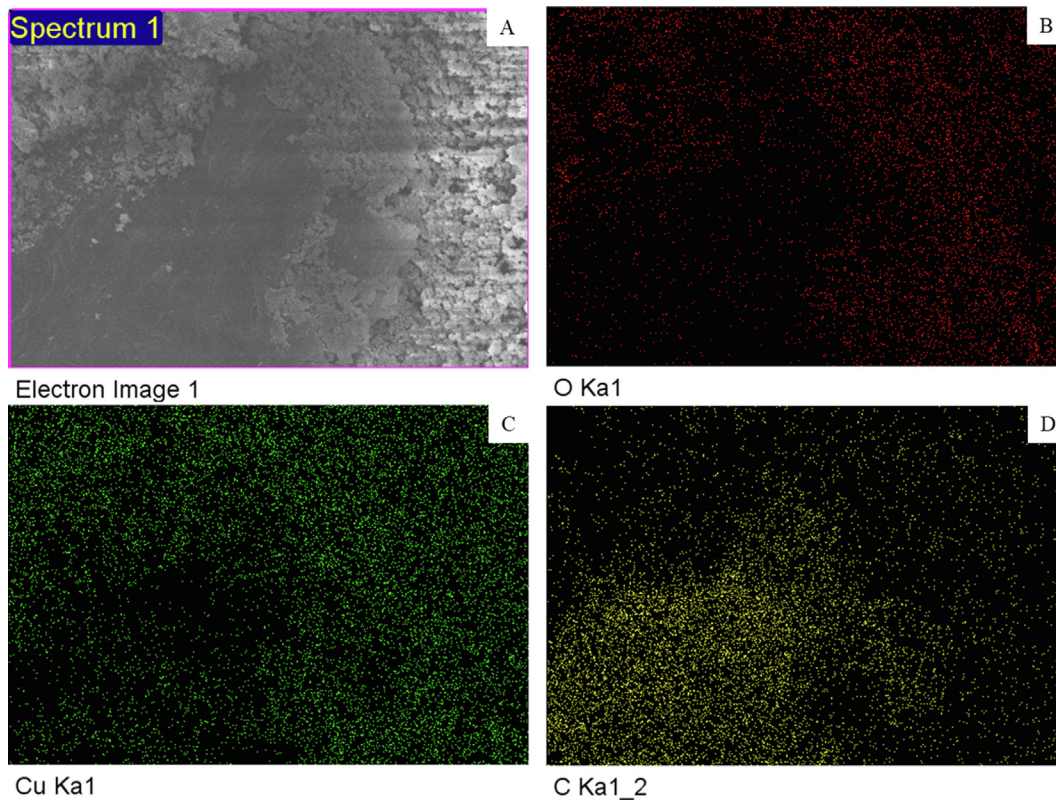
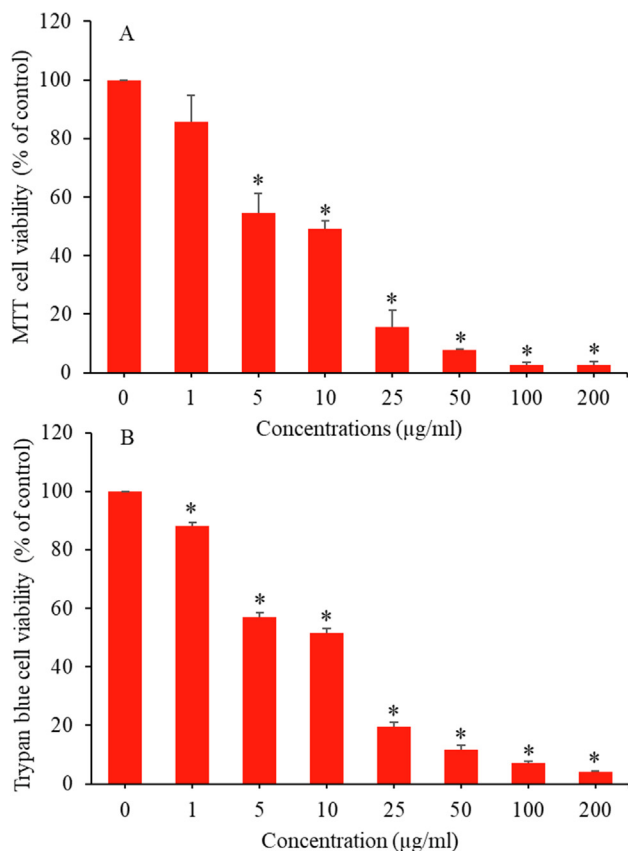


Fig. 3. Elemental mapping of CuO-rGO NCs obtained by EDS associated with FESEM. CuO-rGO NCs: Copper oxide-reduced graphene oxide nanocomposites, EDS: Energy dispersive X-ray spectroscopy, and FESEM: Field emission scanning electron microscopy.



**Fig. 4.** CuO-rGO NCs induced cytotoxicity in NRK52E cells. (A) MTT cell viability assay and (B) trypan blue cell viability assay. Data are presented as mean  $\pm$  SD of three independent experiments ( $n = 3$ ). \*Significantly different from the control ( $p < 0.05$ ). CuO-rGO NCs: Copper oxide-reduced graphene oxide nanocomposites, NRK52E: Normal rat kidney cells, MTT: 3-(4,5-dimethylthiazol-2-yl)-2,5-diphenyltetrazolium bromide, and SD: Standard deviation.

dye passively enters into cells where it reacts with ROS and converted into highly fluorescent molecule DCF. Intracellular intensity of DCF was captured by fluorescent microscope. Fig. 6 indicated that CuO-rGO NCs significantly induce ROS production in NRK52E cells. Fluorescent intensity of DCF (indication of ROS generation) in CuO-rGO NCs treated cells was higher as compared to untreated control cells. CuO-rGO NCs induced ROS generation observed in the present study is comparable to earlier reports of ROS generation and oxidative stress response of pure CuO NPs (Abdelazeim et al., 2020; Ahamed et al., 2015).

### 3.4. Apoptotic response of CuO-rGO NCs

Apoptosis potential of CuO NPs has been reported in several studies (Ahamed et al., 2015). Our previous work also found that CuO NPs induce DNA damage and apoptosis in human liver (HepG2) cells (Siddiqui et al., 2013). Apoptosis response of relative new nanostructures such as metal oxide-graphene derivatives nanocomposites are not explored yet. Cell shrinkage and chromatin condensation are important morphological examination of apoptotic cells (Naz et al., 2020). In this study, chromosomal condensation was examined by DAPI staining in NRK52E following exposure to CuO-rGO NCs for 24 h. Fluorescent micrographs of

DAPI staining demonstrated that CuO-rGO NCs effectively induced chromosomal/nuclear condensation and these phenomena increases with increasing the concentrations (Fig. 7). Apoptotic response of CuO-rGO NCs in NRK52E cells was further investigated using acridine orange/ ethidium bromide (AO/EB) dual staining. Cells were exposed for 24 h with CuO-rGO NCs at the concentrations of 10  $\mu\text{g/ml}$  and 25  $\mu\text{g/ml}$ . AO is a vital dye that penetrates cell nuclei of the both live and dead cells (green color), whereas EB only stain cell nuclei that lost their membrane permeability and emits orange-red fluorescent (Liu et al., 2015). The EB dye binds to concentrated DNA fragments and apoptotic bodies. Cells undergoing apoptosis exhibit condensed chromatin and show orange/red stain (AO/EB dual staining) compared with the live healthy cells that appear green (only AO staining) when observed under fluorescent microscope (Anantharaju et al., 2017). As we can see in Fig. 8 that untreated control cells appear as green without orange-red stain, revealing healthy and live cells. However, exposure of CuO-rGO NCs instigated the appearance of orange-red nuclei in a number of cell population. The number of orange-red stained nuclei increases with increasing concentration of CuO-rGO NCs (Fig. 8).

Cell cycle analysis supports a better understanding of nanomaterial-induced cytotoxicity (Huang et al., 2017). In this study, effect of different concentrations of CuO-rGO NCs (1, 2.5, 5, and 10  $\mu\text{g/ml}$  for 24 h) on cell cycle progression of NRK52E cells was further examined using the PI dye (Fig. 9A–F). The PI measures the DNA content of damaged cells from each phase of cell cycle. Cells contain damaged DNA gather in gap1 (G1), synthesis of DNA (S), or gap2/mitosis (G2/M) phases of cell cycle. Cells that contain irreparable DNA damage undergo apoptosis and accumulate in subG1 phase of cell cycle (Huang et al., 2017). Fig. 9F exhibited that cells exposed to CuO-rGO NCs showed a significant increase in cell population of subG1 phase. The cell population of control group in subG1 phase was 1.13 %, which increases 4.7 %–20 % after the treatment of CuO-rGO NCs (1–10  $\mu\text{g/ml}$ ). Cell population with damaged DNA was also increases in DNA synthesis phase (S) following CuO-rGO exposure. Besides, a significant decline of cell percentage in G1 phase was also noticed after the treatment of CuO-rGO NCs. Cell cycle arrest due to metal oxide NPs including CuO was also reported in earlier studies (Ahamed et al., 2016; Huang et al., 2017). These results indicated the apoptotic potential of CuO-rGO NCs in NRK52E cells.

## 4. Conclusion

CuO-rGO NCs was synthesized by a simple hydrothermal process. XRD, FESEM, and EDS characterization data showed that prepared CuO-rGO NCs were crystalline, polygonal shaped, smooth surface morphology, and uniform distribution of Cu, O, and C elements. CuO-rGO NCs induced a dose-dependent cytotoxicity in NRK52E cells. Intracellular ROS generation following CuO-rGO NCs exposure was also observed. Induction of chromosomal condensation was detected after the treatment of CuO-rGO NCs through DAPI staining. Acridine orange/ ethidium bromide (AO/EB) double staining indicates apoptotic response of CuO-rGO NCs. Cell cycle analysis showed that CuO-rGO NCs induce significantly higher percentage of apoptotic cell population in subG1 phase. Overall, these data showed cytotoxic and apoptotic potential of CuO-rGO NPs in NRK52E cells. This work warranted further research to explore the molecular mechanism of CuO-rGO NCs toxicity at suitable *in vivo* models.

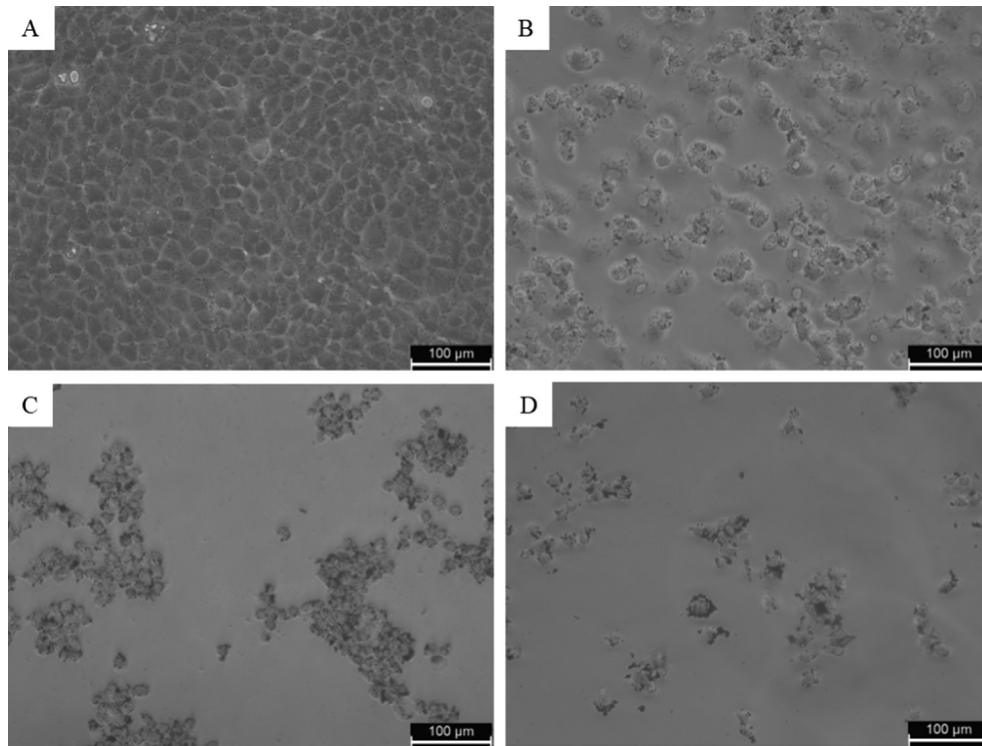


**Fig. 5.** Morphology of NRK52E cells following exposure to CuO-rGO NCs for 24 h. (A) untreated control, (B) cells treated with 25 µg/ml, (C) 50 µg/ml, and (D) 100 µg/ml. NRK52E: Normal rat kidney cells and CuO-rGO NCs: Copper oxide-reduced graphene oxide nanocomposites.

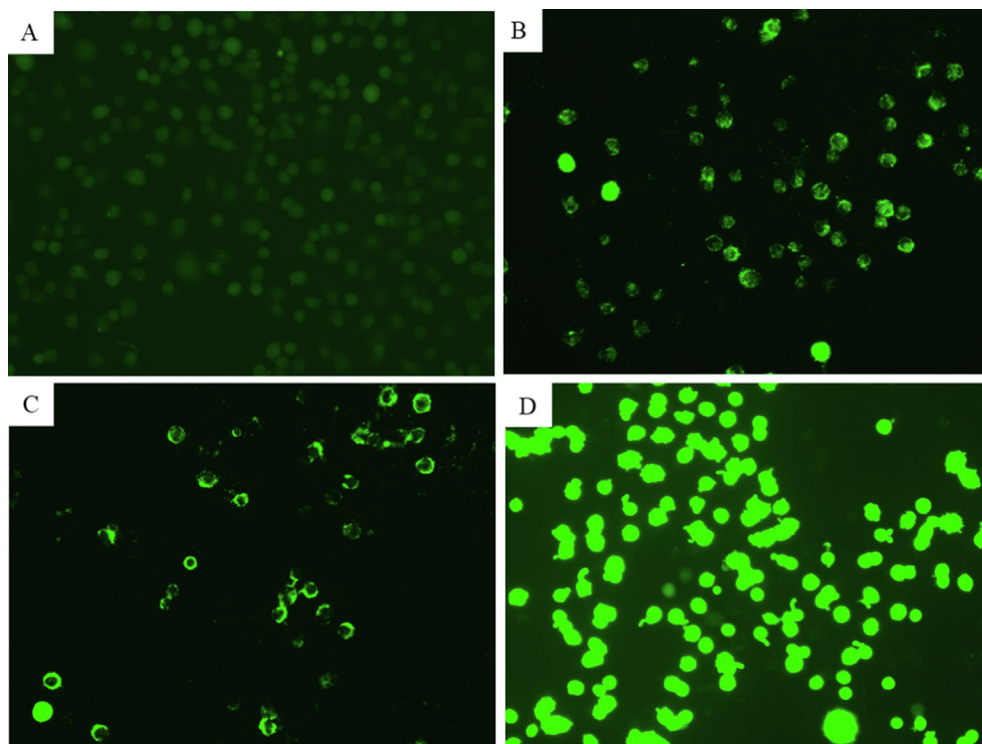


**Fig. 6.** Fluorescence microscopic observation of intracellular ROS generation in NRK52E cells following exposure to different concentrations of CuO-rGO NCs for 24 h. (A) Control cells. (B) Cells treated with 10 µg/ml of CuO-rGO NCs. (C) Cells treated with 25 µg/ml of CuO-rGO NCs. (D) Cells treated with H<sub>2</sub>O<sub>2</sub> for positive control. ROS: Reactive oxygen species, NRK52E: Normal rat kidney cells and CuO-rGO NCs: Copper oxide-reduced graphene oxide nanocomposites, and H<sub>2</sub>O<sub>2</sub>: Hydrogen peroxide.

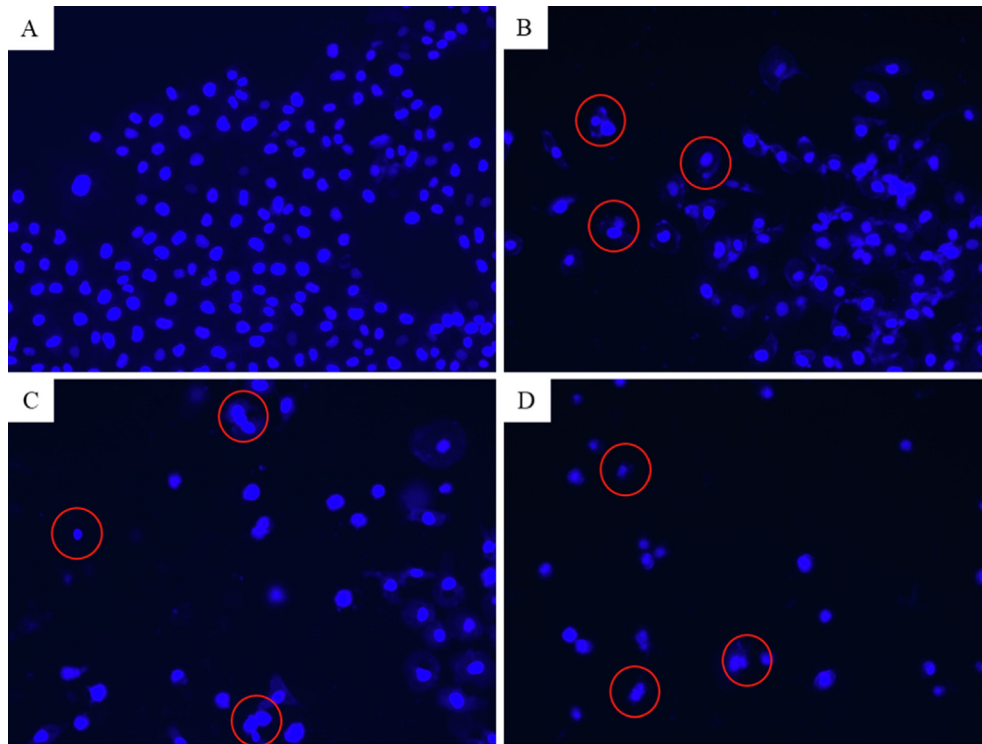


**Fig. 7.** Fluorescence microscopic observation of chromosomal condensation of NRK52E cells following exposure to different concentrations of CuO-rGO NCs for 24 h. (A) Control cells. (B) Cells treated with 25 µg/ml of CuO-rGO NCs. (C) Cells treated with 50 µg/ml of CuO-rGO NCs. (D) Cells treated with 100 µg/ml of CuO-rGO NCs. Red circles indicate chromosomal condensation. NRK52E: Normal rat kidney cells and CuO-rGO NCs: Copper oxide-reduced graphene oxide nanocomposites.

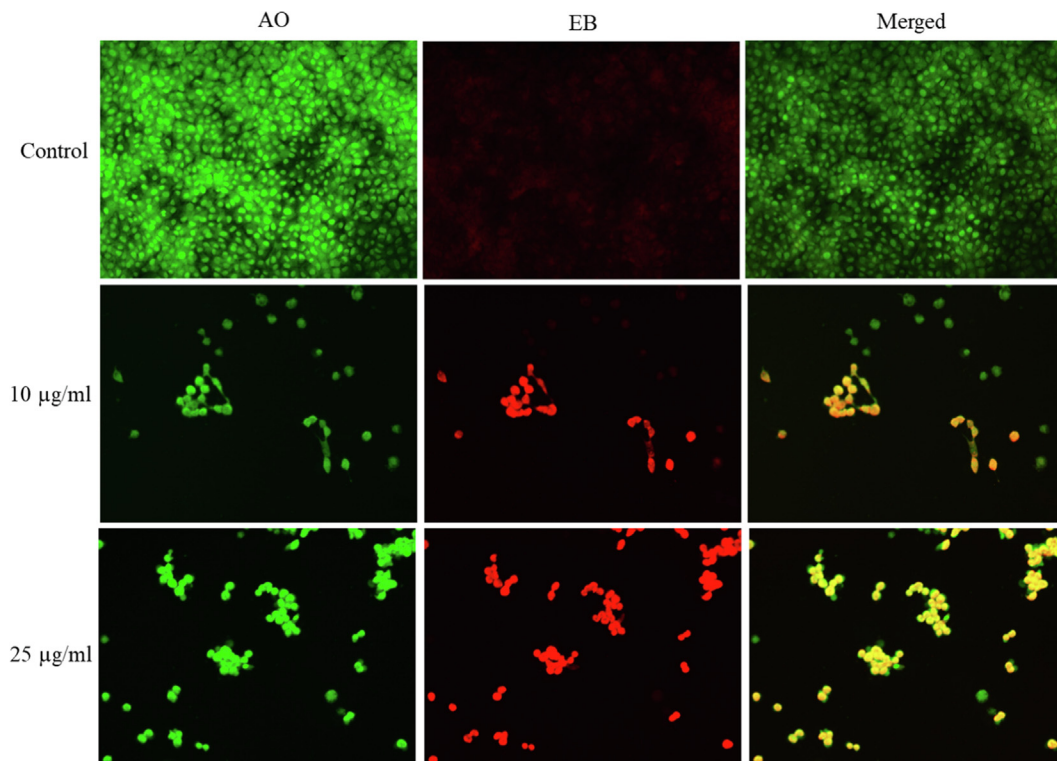


**Fig. 8.** Fluorescence microscopic observation of acridine orange/ethidium bromide (AO/EB) dual staining of NRK52E cells following exposure to different concentrations of CuO-rGO NCs for 24 h. CuO-rGO NCs induced apoptosis in NRK52E cells evident by the presence of orange-red stained cells in treated groups, whereas control cells appears as green. AO/EB: Acridine orange/ethidium bromide, NRK52E: Normal rat kidney cells and CuO-rGO NCs: Copper oxide-reduced graphene oxide nanocomposites.

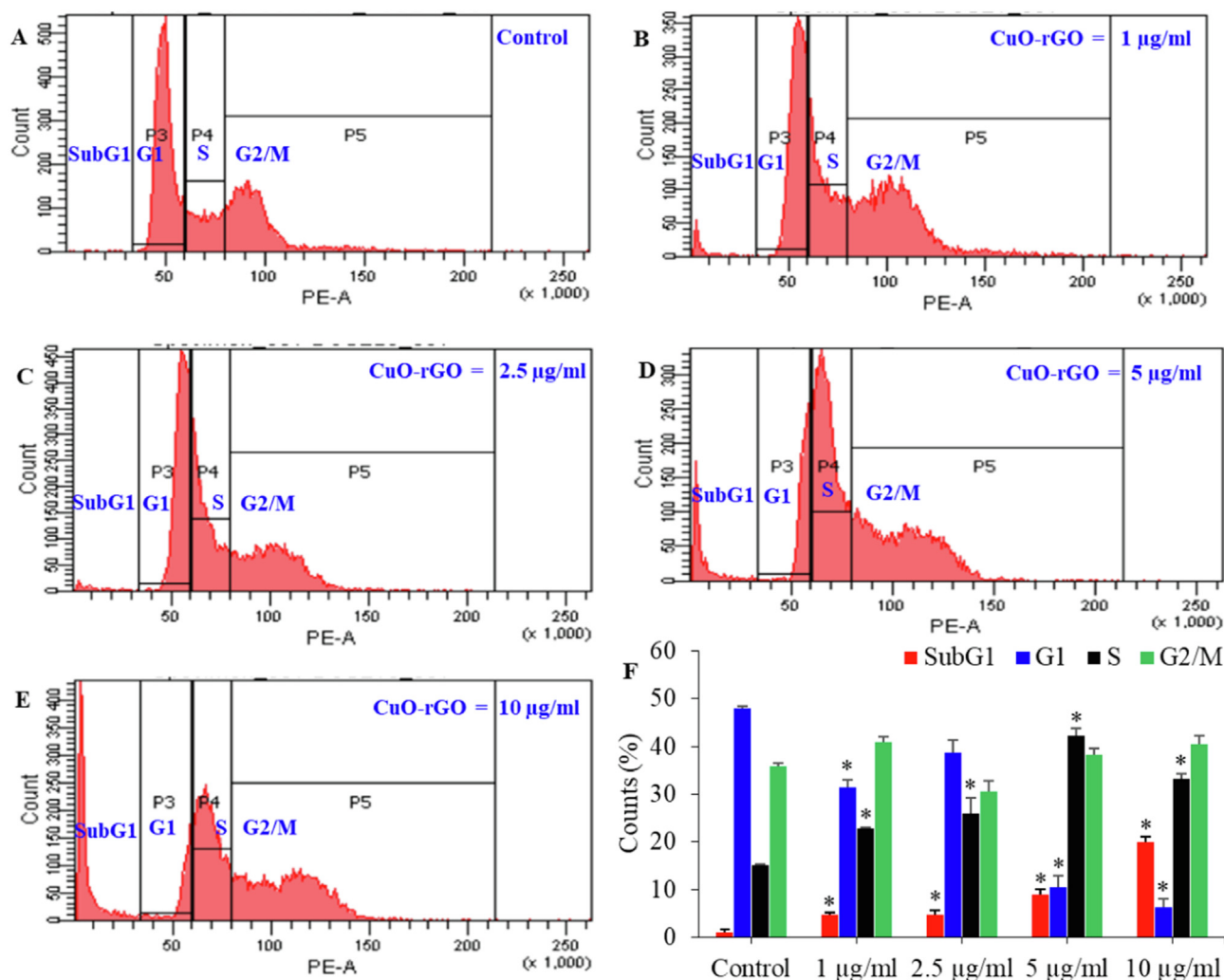


**Fig. 9.** Cell cycle progression of NRK52E cells exposed for 24 h to different concentrations of CuO-rGO (1–10 µg/ml) (A–E). The percentage of cell population in SubG1, G1, S, and G2/M phases were estimated (F). Data are presented as mean  $\pm$  SD of three independent experiments ( $n = 3$ ). \*Statistically significant from the control ( $p < 0.05$ ). NRK52E: Normal rat kidney cells and CuO-rGO NCs: Copper oxide-reduced graphene oxide nanocomposites.

## Declaration of Competing Interest

The authors declare that they have no known competing financial interests or personal relationships that could have appeared to influence the work reported in this paper.

## Acknowledgement

The authors extend their sincere appreciation to the Researchers Supporting Project number (RSP2023R129), King Saud University, Riyadh, Saudi Arabia.

## References

- Abdelazeim, S.A., Shehata, N.I., Aly, H.F., Shams, S.G.E., 2020. Amelioration of oxidative stress-mediated apoptosis in copper oxide nanoparticles-induced liver injury in rats by potent antioxidants. *Sci. Rep.* 10, 1–14. <https://doi.org/10.1038/s41598-020-67784-y>.
- Ahamed, M., Alhadlaq, H.A., Khan, M.A.M., Karupppiah, P., Al-Dhabi, N.A., 2014. Synthesis, characterization, and antimicrobial activity of copper oxide nanoparticles. *J. Nanomater.* 2014, 1–4.
- Ahamed, M., Akhtar, M.J., Alhadlaq, H.A., Alrokayan, S.A., 2015. Assessment of the lung toxicity of copper oxide nanoparticles: current status. *Nanomedicine* 10 (15), 2365–2377.

- Ahamed, M., Akhtar, M.J., Alhadlaq, H.A., Alshamsan, A., 2016. Copper ferrite nanoparticle-induced cytotoxicity and oxidative stress in human breast cancer MCF-7 cells. *Colloids Surf. B Biointerfaces* 142, 46–54.
- Ahamed, M., Akhtar, M.J., Khan, M.M., Alhadlaq, H.A., 2021. SnO<sub>2</sub>-Doped ZnO/Reduced graphene oxide nanocomposites: synthesis, characterization, and improved anticancer activity via oxidative stress pathway. *Int. J. Nanomed.* 16, 89–104. <https://doi.org/10.2147/IJN.S285392>.
- Ahamed, M., Javed Akhtar, M., Majeed Khan, M.A., Alhadlaq, H.A., 2022. Facile green synthesis of ZnO-RGO nanocomposites with enhanced anticancer efficacy. *Methods* 199, 28–36. <https://doi.org/10.1016/j.YMETH.2021.04.020>.
- Anantharaju, P.G., Reddy, B.D., Padukudru, M.A., Kumari Chitturi, C.H.M., Vimalambike, M.G., Madhunapantula, S.V., 2017. Naturally occurring benzoic acid derivatives retard cancer cell growth by inhibiting histone deacetylases (HDAC). *Cancer Biol. Ther.* 18 (7), 492–504.
- Arun, L., Karthikeyan, C., Philip, D., Unni, C., 2020. Optical, magnetic, electrical, and chemo-catalytic properties of bio-synthesized CuO/NiO nanocomposites. *J. Phys. Chem. Solid* 136. <https://doi.org/10.1016/j.jpics.2019.109155>.
- Azam, A., Ahmed, A.S., Oves, M., Khan, M.S., Habib, S.S., Memic, A., 2012. Antimicrobial activity of metal oxide nanoparticles against Gram-positive and Gram-negative bacteria: a comparative study. *Int. J. Nanomed.* 7, 6003–6009. <https://doi.org/10.2147/IJN.S35347>.
- Baeg, E., Sooklert, K., Sereemaspan, A., 2018. Copper oxide nanoparticles cause a dose-dependent toxicity via inducing reactive oxygen species in drosophila. *Nanomaterials* 8 (10), 824.
- Bugata, L.S.P., Pitta Venkata, P., Gundu, A.R., Mohammed Fazlur, R., Reddy, U.A., Kumar, J.M., Mekala, V.R., Bojja, S., Mahboob, M., 2019. Acute and subacute oral toxicity of copper oxide nanoparticles in female albino Wistar rats. *J. Appl. Toxicol.* 39, 702–716. <https://doi.org/10.1002/jat.3760>.
- Cuillet, M., Chevallet, M., Charbonnier, P., Fauquant, C., Pignot-Paintrand, I., Arnaud, J., Cassio, D., Michaud-Soret, I., Mintz, E., 2014. Interference of CuO

- nanoparticles with metal homeostasis in hepatocytes under sub-toxic conditions. *Nanoscale* 6, 1707–1715. <https://doi.org/10.1039/c3nr05041f>.
- Dat, D.Q., Phuong, V.T.L., Van Nang, L., Van Toan, N., Van Duy, N., Duc Hoa, N., 2022. Synthesis of CuO/rGO nanocomposites for carcinogenic Congo red photodegradation. *Adv. Nat. Sci. Nanosci. Nanotechnol.* 12 (4), 045014.
- Fahmy, H.M., Ebrahim, N.M., Gaber, M.H., 2020. In-vitro evaluation of copper/copper oxide nanoparticles cytotoxicity and genotoxicity in normal and cancer lung cell lines. *J. Trace Elem. Med. Biol.* 60, <https://doi.org/10.1016/j.jtemb.2020.126481> 126481.
- Ganesan, K., Jothi, V.K., Natarajan, A., Rajaram, A., Ravichandran, S., Ramalingam, S., 2020. Green synthesis of Copper oxide nanoparticles decorated with graphene oxide for anticancer activity and catalytic applications. *Arab. J. Chem.* 13, 6802–6814. <https://doi.org/10.1016/j.ARABJC.2020.06.033>.
- Ghasemi, M., Turnbull, T., Sebastian, S., Kempson, I., 2021. The mtt assay: Utility, limitations, pitfalls, and interpretation in bulk and single-cell analysis. *Int. J. Mol. Sci.* 22. <https://doi.org/10.3390/IJMS222312827/S1>.
- Huang, Y.-W., Cambre, M., Lee, H.-J., 2017. The toxicity of nanoparticles depends on multiple molecular and physicochemical mechanisms. *Int. J. Mol. Sci.* 18 (12), 2702.
- Islam, M.R., Obaid, J.E., Saiduzzaman, M., Nishat, S.S., Debnath, T., Kabir, A., 2020. Effect of Al doping on the structural and optical properties of CuO nanoparticles prepared by solution combustion method: experiment and DFT investigation. *J. Phys. Chem. Solid* 147, <https://doi.org/10.1016/j.jpics.2020.109646> 109646.
- Laha, D., Pramanik, A., Maity, J., Mukherjee, A., Pramanik, P., Laskar, A., Karmakar, P., 2014. Interplay between autophagy and apoptosis mediated by copper oxide nanoparticles in human breast cancer cells MCF7. *Biochim. Biophys. Acta Gen. Subj.* 1840, 1–9. <https://doi.org/10.1016/j.bbagen.2013.08.011>.
- Liu, K., Liu, P., Cheng, R., Wu, X., 2015. Dual AO/EB staining to detect apoptosis in osteosarcoma cells compared with flow cytometry. *Med. Sci. Monit. Basic Res.* 21, 15. <https://doi.org/10.12659/MSMBR.893327>.
- Mosmann, T., 1983. Rapid colorimetric assay for cellular growth and survival: application to proliferation and cytotoxicity assays. *J. Immunol. Methods* 65, 55–63. [https://doi.org/10.1016/0022-1759\(83\)90303-4](https://doi.org/10.1016/0022-1759(83)90303-4).
- Nayak, R., Ali, F.A., Mishra, D.K., Ray, D., Aswal, V.K., Sahoo, S.K., Nanda, B., 2020. Fabrication of CuO nanoparticle: An efficient catalyst utilized for sensing and degradation of phenol. *J. Mater. Res. Technol.* 9, 11045–11059. <https://doi.org/10.1016/j.jmrt.2020.07.100>.
- Naz, S., Gul, A., Zia, M., 2020. Toxicity of copper oxide nanoparticles: a review study. *IET Nanobiotechnol.* 14 (1), 1–13.
- Padmajan Sasikala, S., Lim, J., Kim, I.H., Jung, H.J., Yun, T., Han, T.H., Kim, S.O., 2018. Graphene oxide liquid crystals: a frontier 2D soft material for graphene-based functional materials. *Chem. Soc. Rev.* 47 (16), 6013–6045.
- Patterson, A.L., 1939. The scherrer formula for X-ray particle size determination. *Phys. Rev.* 56, 978–982. <https://doi.org/10.1103/PhysRev.56.978>.
- Rajapaksha, P., Cheeseman, S., Hombsch, S., Murdoch, B.J., Gangadoo, S., Blanch, E. W., Truong, Y., Cozzolino, D., McConville, C.F., Crawford, R.J., Truong, V.K., Elbourne, Chapman, J., 2019. Antibacterial properties of graphene oxide-copper oxide nanoparticle nanocomposites. *ACS Appl. Bio Mater.* 2, 5687–5696. [https://doi.org/10.1021/ACSABM.9B00754/SUPPL\\_FILE/MT9B00754\\_SI\\_001.PDF](https://doi.org/10.1021/ACSABM.9B00754/SUPPL_FILE/MT9B00754_SI_001.PDF).
- Sarker, P., Sen, S.K., Mia, M.N.H., Pervez, M.F., Mortuza, A.A., Hossain, S., Mortuza, M. F., Ali, M.H., Nur, S., Kabir, H., Chowdhury, M.A.M., 2020. Effect of gamma irradiation on structural, morphological and optical properties of thermal spray pyrolysis deposited CuO thin film. *Ceram. Int.* 47 (3), 3626–3633.
- Sárközy, M., Kovács, Z.Z.A., Kovács, M.G., Gáspár, R., Szűcs, G., Dux, L., 2018. Mechanisms and modulation of oxidative/nitrative stress in Type 4 cardio-renal syndrome and renal sarcopenia. *Front. Physiol.* 9, 1648. <https://doi.org/10.3389/fphys.2018.01648>.
- Shewale, P.S., Yun, K.S., 2020. Synthesis and characterization of Cu-doped ZnO/RGO nanocomposites for room-temperature H<sub>2</sub>S gas sensor. *J. Alloy. Compd.* 837, <https://doi.org/10.1016/j.jallcom.2020.155527> 155527.
- Siddique, S., Zain-ul-Abdin, Waseem, M., Naseem, T., Bibi, A., Hafeez, M., Din, S.U., Haq, S., Qureshi, S., 2021. Photo-Catalytic and anti-microbial activities of rGO/CuO nanocomposite. *J. Inorg. Organomet. Polym.* 31 (3), 1359–1372.
- Siddiqui, M.A., Alhadlaq, H.A., Ahmad, J., Al-Khedhairi, A.A., Musarrat, J., Ahamed, M., Pant, A.B., 2013. Copper oxide nanoparticles induced mitochondria mediated apoptosis in human hepatocarcinoma cells. *PLoS One* 8 (8), e69534.
- Sruthi, S., Ashtami, J., Mohanan, P.V., 2018. Biomedical application and hidden toxicity of Zinc oxide nanoparticles. *Mater. Today Chem.* 10, 175–186. <https://doi.org/10.1016/j.MTCHEM.2018.09.008>.
- Strober, W., 2015. Trypan blue exclusion test of cell viability. *Curr. Protoc. Immunol.* 111 (1).
- Wang, H., Joseph, J.A., 1999. Quantifying cellular oxidative stress by dichlorofluorescein assay using microplate reader. *Free Radic. Biol. Med.* 27, 612–616. [https://doi.org/10.1016/S0891-5849\(99\)00107-0](https://doi.org/10.1016/S0891-5849(99)00107-0).
- Wu, F., Harper, B.J., Crandon, L.E., Harper, S.L., 2020. Assessment of Cu and CuO nanoparticle ecological responses using laboratory small-scale microcosms. *Environ. Sci. Nano* 7, 105–115. <https://doi.org/10.1039/c9en01026b>.
- Xu, J., Zhang, Q., Li, X., Zhan, S., Wang, L., Chen, D., 2017. The effects of copper oxide nanoparticles on dorsoventral patterning, convergent extension, and neural and cardiac development of zebrafish. *Aquat. Toxicol.* 188, 130–137. <https://doi.org/10.1016/j.aquatox.2017.05.002>.
- Yang, Z., Xiao, Y., Jiao, T., Zhang, Y., Chen, J., Gao, Y., 2020. Effects of copper oxide nanoparticles on the growth of rice (*Oryza sativa* L.) seedlings and the relevant physiological responses. *Int. J. Environ. Res. Public Health* 17 (4), 1260.
- Zhang, D., Yin, N., Jiang, C., Xia, B., 2016. Characterization of CuO-reduced graphene oxide sandwiched nanostructure and its hydrogen sensing characteristics. *J. Mater. Sci.: Mater. Electron* 28 (3), 2763–2768.
- Zhang, J., Zou, Z., Wang, B., Xu, G., Wu, Q., Zhang, Y., Yuan, Z., Yang, X., Yu, C., 2018. Lysosomal deposition of copper oxide nanoparticles triggers HUVEC cells death. *Biomaterials* 161, 228–239. <https://doi.org/10.1016/j.biomaterials.2018.01.048>.